Study of phase changes of the water octamer using parallel tempering and multihistogram methods

Pablo Nigra, Marcelo A. Carignano, and Sabre Kais[a)]
Department of Chemistry, Purdue University, West Lafayette, Indiana 47907

(Received 24 April 2001; accepted 25 May 2001)

Parallel tempering Monte Carlo and multihistogram methods are combined to study the phase changes of the water octamer. The heat capacity is calculated continuously from very low temperatures up to $T=230$ K. We find the melting temperature to be 178.5 K. In addition, a solid–solid phase change is found at 12 K. We introduce an order parameter to monitor this low temperature phase change. © *2001 American Institute of Physics.* [DOI: 10.1063/1.1385795]

I. INTRODUCTION

The study of molecular clusters has attracted considerable attention in the recent years. These systems exhibit phase change properties; some of which are very unique to finite systems, and others that correlate in bulk matter. The size of the system is small enough to allow a detailed study of its structural and thermodynamic properties.[1–8] In particular, water cluster properties and their dependence on the number of molecules can give us new insights into the rich phase behavior of water.

The water octamer is a small molecular cluster that presents a well-established melting phase change when described by several known potential models.[9–14] The melting region can be readily traced by searching for a peak in the curve of the heat capacity versus temperature: the energy distribution function $w(\epsilon)$ is neatly bimodal.[9] Below the melting region, the solidlike phases consist of several cubic forms of which the isomers D_{2d} and S_4 are the main components. In the melting region, cubic and open forms coexist altogether. Finally, above the melting region, the liquidlike phase is composed of a wide variety of opened structures.[10]

The isomers D_{2d} and S_4 belong to the two lowest lying energy minima. Both *ab initio* and density functional calculations signal the D_{2d} structure to correspond to the global minimum.[15–18] Nevertheless, some recent density functional calculations point out that the stabilization order is reversed when zero point energy corrections are included.[19,20] From the experimental side, there is conclusive evidence for the existence of the structures D_{2d} and S_4, as well as another low lying cubic structure whose point group symmetry is C_i.[19,21,22]

Associated with the melting process, there is a high energy barrier separating the solidlike and liquidlike phases. Energy barriers cause ergodicity breaking during simulations. In particular, standard Metropolis Monte Carlo suffers the ergodicity breaking in a way that makes it very difficult to estimate simple averages with any accuracy in a reasonable computational time.[10,11] Suitable techniques have been developed in the last few years to fix this problem; for example, jump–walking Monte Carlo.[23] This method has been used to study the canonical heat capacity of the water octamer in the melting region.[9–11]

In the present work, we revisit the water octamer to investigate the behavior of the canonical properties from very low temperatures up to the melting region. To that end, we apply an alternative technique named parallel tempering Monte Carlo which is similar in spirit to the jump–walking algorithm.[24,25] The parallel tempering method has been recently used to characterize the phase changes in the systems LJ_{38} and Ar_N-HF.[26–29] Here, we combine parallel tempering Monte Carlo with the multihistogram algorithm to cover continuously the whole range of temperatures.

We describe now the organization of this paper. In Sec. II we introduce the model potential for the water octamer. In Sec. III we describe our implementation of the parallel tempering algorithm. In Sec. IV we report properties related to the Monte Carlo dynamics such as the autocorrelation function $\gamma(t)$ and the integrated correlation time τ. In Sec. V we show the canonical heat capacity $c_v(T)$. In Sec. VI we present results of an order parameter for the water octamer. Finally, in Sec. VII we give the conclusions.

II. CLUSTER MODEL

We model the cluster by adopting a rigid molecule scheme for the water molecules. Then, the general form for the total potential energy is given by

$$U=\sum_{i<j}^{N} U^{\mathrm{MCY}}(\mathbf{r}_{ij})+\sum_{i=1}^{N} U^{c}(\mathbf{r}_i), \tag{1}$$

where $\mathbf{r_{ij}}$ represent the distance between molecules i and j, and $\mathbf{r_i}$ is the position of the center of mass of molecule i. We have adopted the well-known MCY potential[30] for the water–water interactions. The external potential U^c has been introduced to prevent evaporation in the simulations at the higher temperatures. We have adopted a reflecting constraint potential with a radius of $r_c=7$ Å:

$$U^{c}(\mathbf{r})=\begin{cases} 0 & |\mathbf{r}-\mathbf{r}_{\mathrm{c.m.}}|<r_c, \\ \infty & |\mathbf{r}-\mathbf{r}_{\mathrm{c.m.}}|>r_c. \end{cases} \tag{2}$$

Here, $\mathbf{r}_{\mathrm{c.m.}}$ is the center of mass of the cluster.

a)Author to whom correspondence should be addressed. Electronic mail: kais@power1.chem.purdue.edu

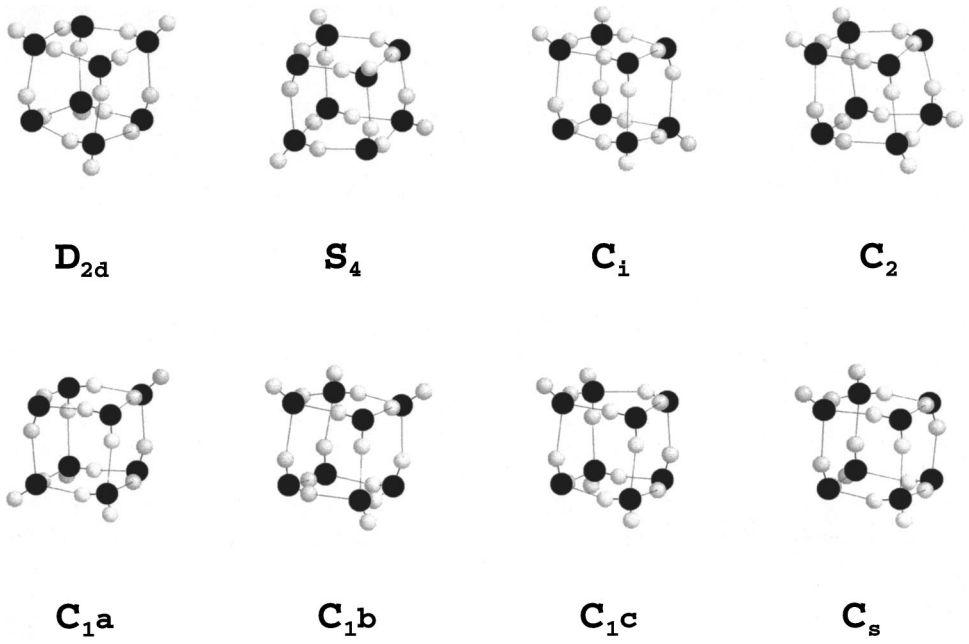

FIG. 1. All the cubic lowest lying energy isomers of the water octamer for the MCY potential. The symbols denote the point group symmetries. The energies of these structure are given in Table II.

III. THE PARALLEL TEMPERING METHOD

The parallel tempering method was originally used in simulations of glassy systems like spin glasses and random fields.[24,25] It has been devised to solve the problems of ergodicity breaking that these systems exhibit at the low temperature regime.

The basic idea of the parallel tempering method is to run simultaneously several simulations at different temperatures using Markovian dynamics and, in addition, let the simulations swap states according to the following probability:

$$p=\min\{1,\exp[(\beta_i-\beta_j)(U_i-U_j)]\}, \tag{3}$$

where U_i is the energy of the state i, and β_i is the inverse temperature $1/k_BT_i$ with k_B being the Boltzmann constant. At least one of the T_i must be high enough to keep the system above all the energy barriers that might cause ergodicity breaking. It has been proven that this combination satisfies both ergodicity and detailed balance.[25]

In the present work, we let the system move using the Metropolis algorithm.[31] Also, a swap between systems with adjacent temperatures was attempted with a frequency $\nu=0.1$; i.e., one swap attempt every 10 Monte Carlo steps.

A Monte Carlo step is defined by N^2 attempts to displace and rotate every water molecule in turn. Therefore, we define the unit time by $\delta t=N^2$. The system is sampled at every Monte Carlo step.

We fix the respective acceptance ratios for displacements and rotations at 0.5 each so that half of the attempts are accepted for both kind of movements.[32] Also, we choose the temperatures of the simulations in order to guarantee the acceptance of at least 10% of the attempted swaps. This can be achieved by letting the energy histograms of adjacent simulations overlap substantially with each other, as inferred from Eq. (3).

To equilibrate the system at each temperature, we initially run the simulations for 1.5×10^6 Monte Carlo steps. In all cases, the initial configurations are that of the global minimum. Next, we sample the system running the simulations for 10^7 Monte Carlo steps.

The global minimum for the MCY–water octamer corresponds to the the D_{2d} isomer shown in Fig. 1. In this figure, we also show all the cubic low lying energy isomers.

On completion of the simulations, we apply the multihistogram algorithm to estimate the heat capacity in the whole range of temperatures.[33] This algorithm combines the results of all the simulations to obtain the best estimates at temperatures other than the temperatures of the simulations. A required condition in common with the parallel tempering method is that adjacent energy histograms must overlap to some degree with each other.

IV. ENERGY HISTOGRAMS, AUTOCORRELATION FUNCTION, AND INTEGRATED CORRELATION TIME

Figure 2 shows the normalized energy histograms $w(\varepsilon)$, where $\varepsilon=U/N$. The numbers indicate the simulation temperatures. Overlap is observed between all neighboring histograms, as required by the parallel tempering method. Some of the histograms are bimodal. This is a characteristic of solid–liquid phase changes.[8]

The energy autocorrelation function $\gamma(t)$ is defined as

$$\gamma(t)=\frac{\langle\varepsilon(0)\varepsilon(t)\rangle-\langle\varepsilon\rangle^2}{\langle\varepsilon^2\rangle-\langle\varepsilon\rangle^2}, \tag{4}$$

where t is the Monte Carlo time measured in δt units. The effect of parallel tempering on $\gamma(t)$ as compared with standard Metropolis simulations is shown in Fig. 3 for a few temperatures in the melting region. In that region, the system is known to fluctuate between the closed cubic forms shown in Fig. 1 and a wide variety of open forms.[9–11,14] It is evident from Fig. 3 that parallel tempering alleviates sensibly the effects of correlations. However, we observed that correlations continue having the same qualitative behavior as in the

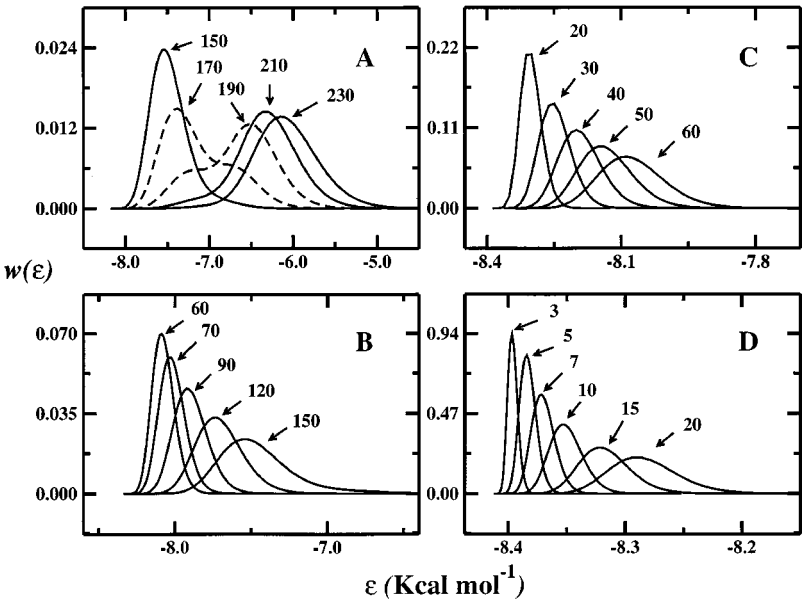

FIG. 2. Normalized histograms $\omega(\varepsilon)$. The numbers are the temperatures in Kelvin, and the energy ε is in Kcal mol^{-1}. The dashed line curves are bimodal. Also, the histograms at $T=150$ and 210 show some bimodality.

cases of simulations without parallel tempering. That is, correlations still become larger in the phase change region. This qualitative agreement is expected since our parallel tempering implementation uses the Metropolis algorithm; the one responsible for the large correlations.[25]

We remark on the shape of $\gamma(t)$ in the melting region. First, it decreases very fast; then, it suddenly levels off to continue decreasing steadily in most cases at a very low rate for a long period. This sort of shape presages large correlations because the more $\gamma(t)$ delays becoming a random number fluctuating around zero, the larger the correlation block of consecutively sampled energies is.[34]

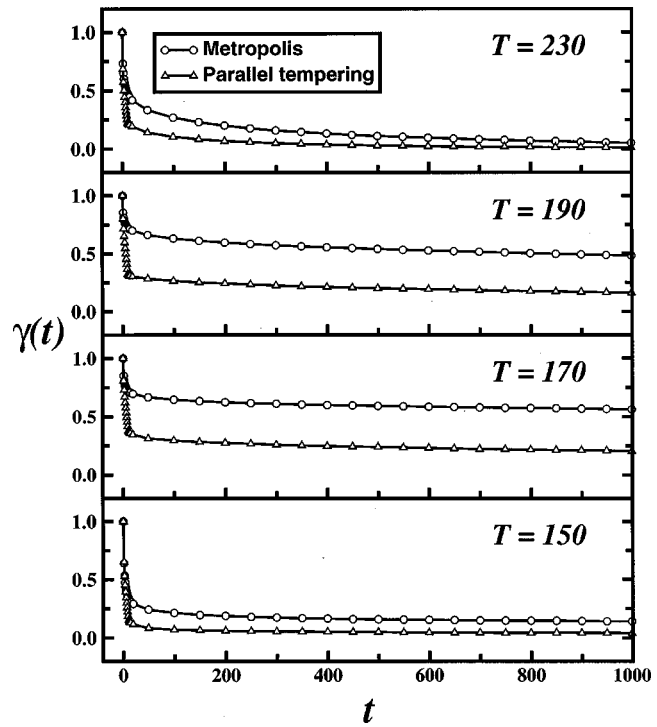

FIG. 3. Comparison of the energy autocorrelation function $\gamma(t)$ for Metropolis and parallel tempering simulations at different temperatures in the melting region. All the temperatures are in Kelvin.

In Fig. 4 we compare the behavior of $\gamma(t)$ for different temperatures. The upper (lower) panel corresponds to temperatures in (below) the melting region. It is observed that $\gamma(t)$ reaches a value which is 10 times larger in the melting region than at lower temperatures. We also note that all the curves sharply level off at approximately the same time.

A way to quantify the correlations in the simulations is by estimating the *integrated* correlation time τ which is defined as[34]

$$\tau=\int_0^\infty \gamma(t)dt. \tag{5}$$

The estimates of τ enter as input in the multihistogram algorithm, which we use in Sec. V to estimate the heat capacity. Also, the values of τ can provide us with some indication of possible phase changes.

The direct calculation of τ by integrating $\gamma(t)$ in Eq. (5) is not practical because it involves evaluating a truncated summation which in turn introduces uncertainties that are difficult to assess. The conventional way then to estimate τ is by first calculating the standard deviation or variance σ of the mean energy of a simulation.

In this work, we use two methods to estimate σ: the blocking method and the moving block bootstrap algorithm.[35,36] Both algorithms consider the sampled energies as a large block and estimate an initial σ. Next, the algorithms transform the original block into a new block and estimate σ once more. Then, the last step is repeated until the estimated σ reaches a steady value. Exactly how the transformations are done and how σ is estimated at every stage depend on each particular method.

It is worthwhile to mention here that the moving block bootstrap algorithm usually gives better estimates of σ than the blocking method at the phase transition region in Ising systems, even though the blocking method is much more

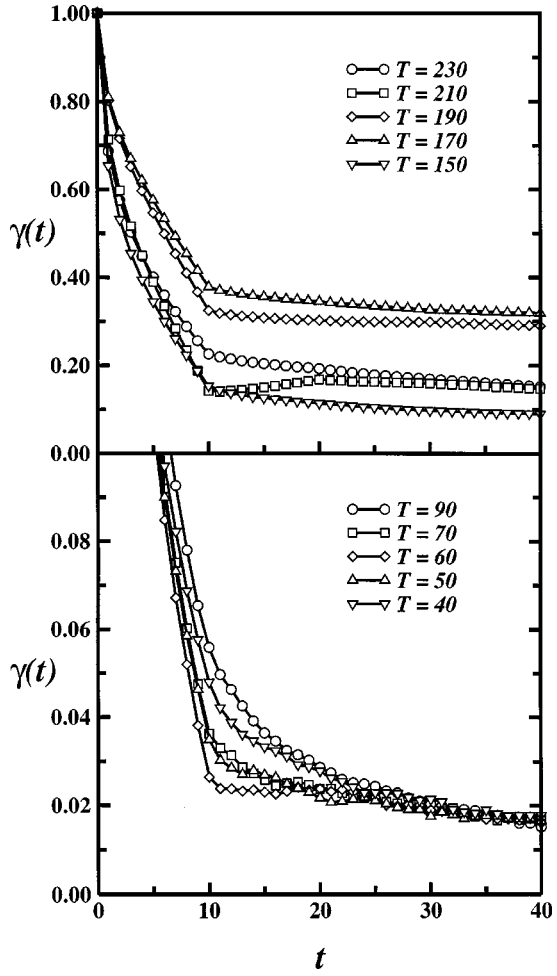

FIG. 4. Parallel tempering energy autocorrelation function $\gamma(t)$ for temperatures in the melting region (upper panel) and for temperatures out of the melting region (lower panel). All the temperatures are in Kelvin.

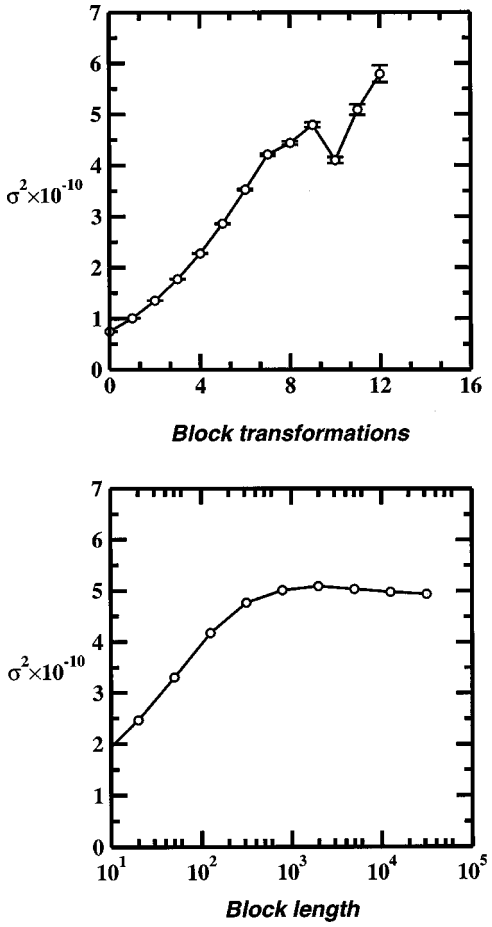

FIG. 5. Square of the energy variance σ^2 at 3 Kelvin calculated by means of both the blocking method (upper panel) and the bootstrap method (lower panel). The units of σ are (Kcal mol^{-1}). Note how, in this case, the bootstrap implementation as in Ref. 36 tends to form a steady plateau (lower panel), in contrast to the blocking implementation of Ref. 35 which fluctuates around some unclear value (upper panel).

efficient. Away from the phase transition region the blocking method is usually the better option because of its efficiency.[36] We find, however, that at a temperature as low as 3 K where the magnitude of correlations is small in comparison with the same magnitude in the melting region, the moving block bootstrap algorithm still may yield better results than the blocking method. This is shown in Fig. 5.

To estimate τ at each temperature, we use the following formula:[34]

$$\sigma^2 = \sigma_0^2 \frac{g(\tau)}{t_{\max}} \tag{6}$$

with

$$\sigma_0^2 = \langle \varepsilon^2 \rangle - \langle \varepsilon \rangle^2, \tag{7}$$

where $t_{\max}$ is the simulation length, and $g(\tau)$ is given by

$$g(\tau) = 1 + 2\tau. \tag{8}$$

Table I shows τ for the different temperatures. As expected from Figs. 3 and 4, τ increases within the melting region, and the increase is much more pronounced for simulations using only Metropolis algorithm. In general, Metropolis simulations in the melting region require a very long computational time to produce results with some accuracy. This is a consequence of the ergodicity breaking caused by high energy barriers. Our results in Fig. 3 and Table I reflect that situation.

Outside the melting region, τ appears to have another maximum around $T=60$, but it is much less noticeable. That region, shown in Sec. VI, corresponds to a system fluctuating between the two solidlike phases D_{2d} and and S_4, see Fig. 1. As the temperature continues decreasing, τ becomes even smaller until it finally stabilizes in a region below $T=20$, see Table I. That last region corresponds to a single solidlike phase in the global minimum basin.

TABLE I. Estimates of the integrated correlation time τ. The values in parentheses correspond to simulations using only the Metropolis algorithm.

T/K	τ	T/K	τ	T/K	τ
230	(173) 53	90	112	20	3
210	(1137) 168	70	116	15	2
190	(2881) 652	60	153	10	2
170	(8475) 1242	50	90	7	2
150	(1736) 269	40	77	5	2
120	66	30	2	3	3

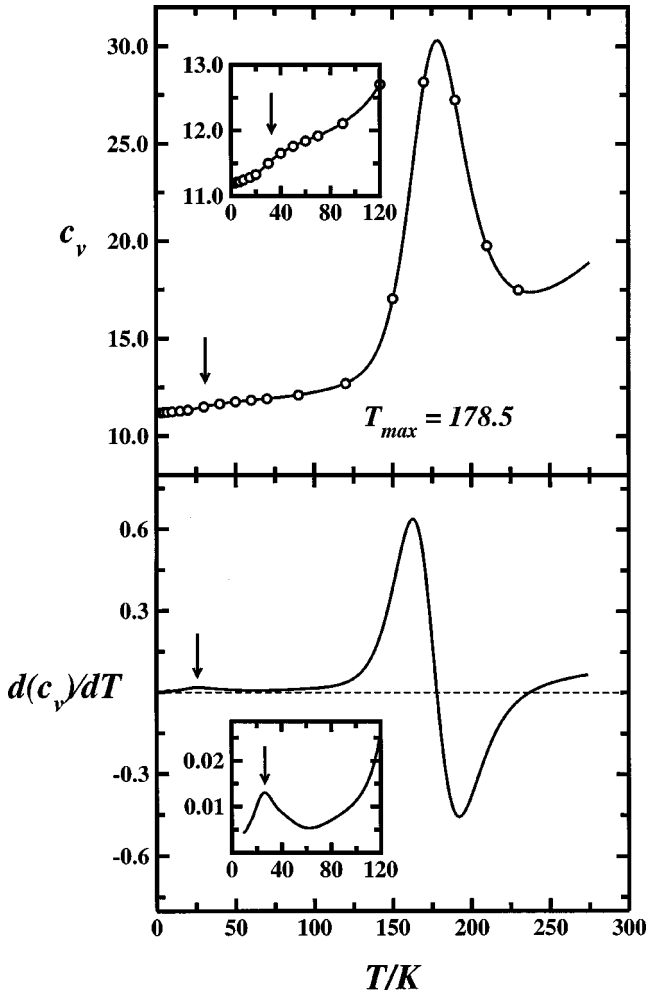

FIG. 6. The heat capacity c_v in Kcal mol^{-1} K^{-1} and its derivative as a function of temperature. The circles corresponds to the simulated values. The solid lines are drawn by using the multihistogram algorithm. The statistical errors are smaller than the width of the line.

V. THE HEAT CAPACITY

The heat capacity per molecule $c_v(T)$ for a system composed of N equal rigid molecules is expressed as

$$c_v(T)=3k_B+Nk_B\beta^2\sigma_0^2, \tag{9}$$

where σ_0^2 is defined in Eq. (7). To estimate $c_v(T)$ and the other thermodynamic functions at temperatures different from those of the simulations, we use the multihistogram algorithm.[33] Figure 6 displays the heat capacity $c_v(T)$ and its derivative with respect to the temperature. The peak in the heat capacity corresponds to the solid–liquid transition. We characterize the temperature of the transition by the temperature of the maximum in the heat capacity. We find a value of $T_{\max}=178.5$ K, which is in reasonable agreement with the value obtained by Pedulla and Jordan.[11]

At lower temperature (20–90 K), we observe the formation of a shoulder in $c_v(T)$ indicated by an arrow. The presence of the shoulder is further confirmed by a small maximum in dc_v/dT. In addition, we note that the position of the shoulder is consistent with the second region of increasing correlation signaled by τ in Table I.

It is desirable to know which cubic isomers take part in the solid–solid phase change. To that end, we introduce an order parameter able to characterize this phase change.

VI. THE ORDER PARAMETER

To define an order parameter, we look for a quantity that is well defined in every state in the phase space of the water octamer. An order parameter should be able to distinguish among the different phases that the system has.[8] To recognize a phaselike form, the order parameter must also be a rotational invariant, i.e., independent of the configurational orientation. For instance, the polarization vector $\mathbf{P}$ is well defined for every state in the phase space, but it is not invariant under rotation. Moreover, its expectation value $\langle\mathbf{P}\rangle$ is identically zero in the whole range of temperatures. Instead, the polarization norm $|\mathbf{P}|$ is an invariant under rotation, and its expectation $\langle|\mathbf{P}|\rangle$ seems likely to distinguish between solidlike and liquidlike phases. Unfortunately, $|\mathbf{P}|$ vanishes by symmetry for the isomers D_{2d} and S_4 shown in Fig. 1. Therefore, $|\mathbf{P}|$ is not appropriate for distinguishing between those isomers.

In this section, we study the properties of an order parameter originally introduced by Steinhardt *et al.* for Lennard-Jones bulk phases.[37] They have developed two sets of rotational invariants based on spherical harmonics labeled Q_l and W_l. Subsequent works on Lennard-Jones clusters have also made use of Q_l and W_l.[26,27,38,39] Since Q_4 has given good results for Lennard-Jones clusters, we will focus our attention on this particular order parameter.

Q_4 is defined by associating a set of spherical harmonics with every bond joining an atom to its near neighbors. The word *bond* here does not necessarily imply chemical bonds, but rather lines connecting pairs of predefined near neighbor atoms. Then, the definition of Q_4 is[37]

$$Q_4=\left(\frac{4\pi}{9}\sum_{m=-4}^{4}|\overline{Q}_{4,m}|^2\right)^{1/2} \tag{10}$$

with

$$\overline{Q}_{4,m}=\frac{1}{n_b}\sum_{r_{ij}}Y_{4,m}(\theta_{ij},\phi_{ij}), \tag{11}$$

where n_b is the number of bonds, $Y_{4,m}(\theta_{ij},\phi_{ij})$ is a spherical harmonic, and θ_{ij} and ϕ_{ij} are the polar and azimuthal angles, respectively, of a vector that points from the mass center of the cluster to the midpoint of the nth bond. We have investigated different choices for the bonds, and have found that they all yield similar information. The results presented here were obtained using the hydrogen–oxygen bond.

The algorithm to find the bonds is as follows: (1) pick a water molecule j and calculate the distances $r_{\alpha_j,i}$ from hydrogen α_j to the oxygens i belonging to other molecules; (2) look for the smallest of the $r_{\alpha_j,i}$ to decide whether hydrogen α_j is bonding or not; (3) continue with the other hydrogen of molecule j,β_j; and (4) repeat all the steps for each of the remaining molecules.

The most sensitive part of this algorithm is the decision whether a hydrogen is bonding or dangling. Considering r_{α_j,i_0} as being the smallest distance, step (2) is achieved by

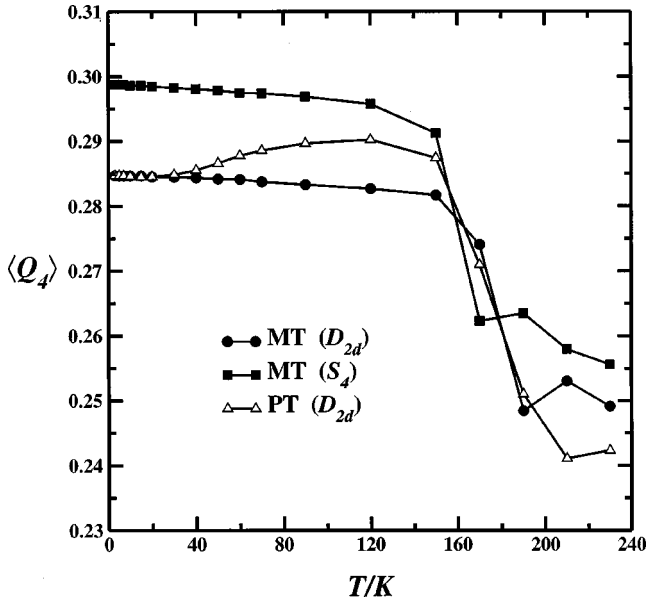

FIG. 7. Expectation value $\langle Q_4 \rangle$ for the hydrogen bonds as a function of the temperature. MT means Metropolis, and PT means parallel tempering. The initial structure is shown in parentheses. See also Table II.

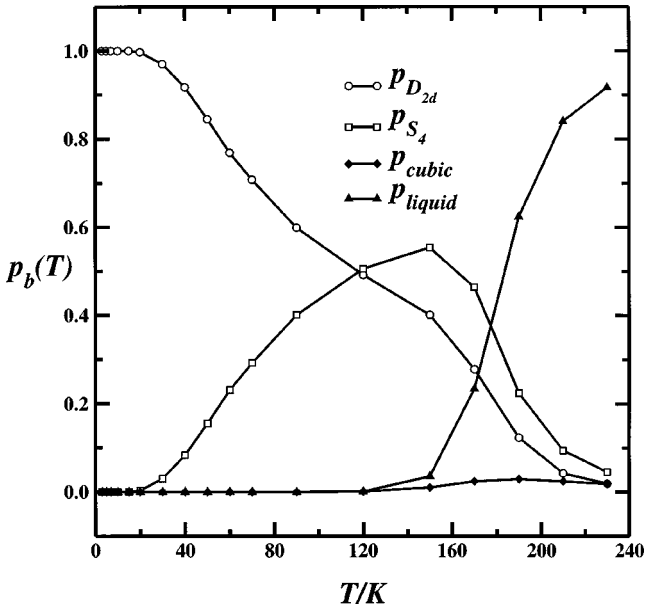

FIG. 8. Probability $p_b(T)$ that a particular basin or group of basins are visited.

executing the following sentences: (a) if $r_{\alpha_j,i_0} > r_{\beta_j,i_0}$, then hydrogen α_j dangles; (b) if step (a) is false, and $r_{\alpha_j,i_0} > (r^2_{j,i_0} + r^2_{\alpha_j,j})^{1/2}$, then hydrogen α_j dangles; and (c) if steps (a) and (b) are false, then hydrogen α_j bonds with oxygen i_0. Here, r_{j,i_0} is the distance from oxygen j to oxygen i_0, and $r_{\alpha_j,j}$ is the distance from hydrogen α_j to its father oxygen j.

Figure 7 shows $\langle Q_4 \rangle$ as a function of the temperature for the parallel tempering simulation and for regular Metropolis simulations seeded with the D_{2d} and S_4 structures. Table II gives the values of Q_4 for the cubic structures in Fig. 1. For the standard Monte Carlo, we see that Q_4 remains almost constant until the melting region is reached. This is because the systems are trapped in the basins of the initial configurations. However, Q_4 for parallel tempering simulations displays the transition from a pure D_{2d} state, to a mixture of cubic structures in the temperature range 15–120 K. For larger temperatures, Q_4 decreases monotonically due to contribution from open structures.

The information provided by Q_4 is complemented by Fig. 8, where we plot the probability $p_b(T)$ that a particular basin or group of basins are visited. This probability is obtained by periodic quenching. Up to $T=10$ K, we have that $p_{D_{2d}}=1$. At $T=15$ K, traces of the S_4 state are observed. An exchange between these two structures occur up to $T=50$ K, where the appearance of the other cubic forms is detected. The first open, or liquidlike structure, is observed at $T=90$ K. However, the number of open structures is insignificant up to $T=120$ K. At the position of the peak in the heat capacity c_v, $T=178.5$ K, the distribution of structures is almost even between cubic and open forms. At higher temperatures, p_{liquid} becomes dominant.

We note that $\langle Q_4 \rangle$ lets us estimate the onset of the first phase change at low temperature. In Fig. 9, we show the result of applying the multihistogram method to the parallel tempering simulations, as well to the Metropolis simulation

TABLE II. Energy per molecule ε and order parameter Q_4 for the cubic structures of Fig. 1.

Structure	ε/Kcal mol^{-1}	Q_4
D_{2d}	−8.413	0.285
S_4	−8.380	0.299
C_2	−8.159	0.323
C_i	−8.127	0.336
C_1b	−8.084	0.303
C_1c	−8.066	0.312
C_1a	−8.052	0.316
C_s	−8.039	0.317

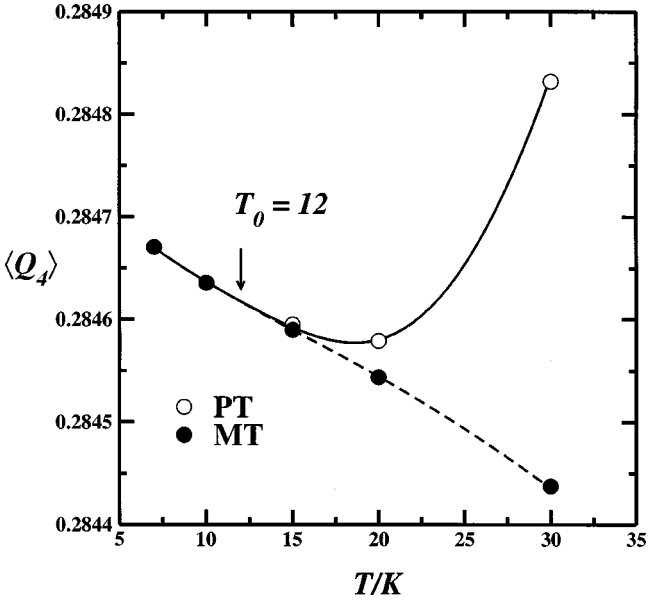

FIG. 9. The same as Fig. 7. The arrow signals the onset temperature T_0.

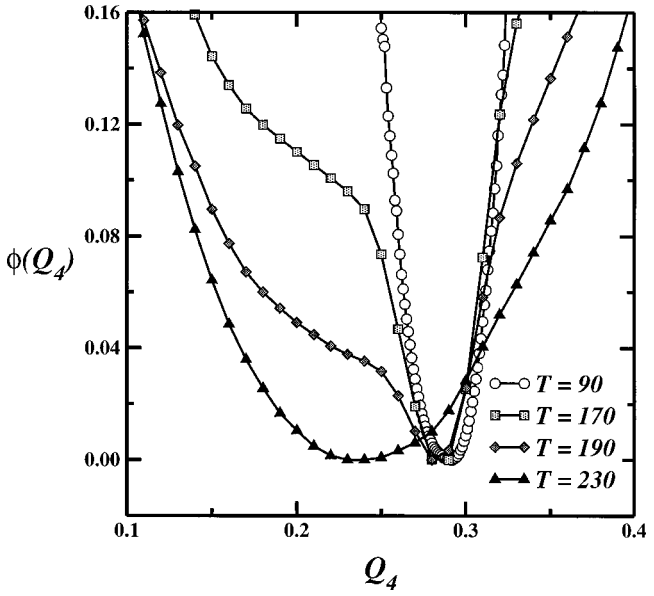

FIG. 10. Landau free energy $\phi(Q_4)$ in Kcal mol^{-1}.

seeded with the D_{2d} structure in the vicinity of $T=15$ K. The point where the two curves meet indicates the temperature, T_0, at which the phase change begins to happen, i.e., where the first S_4 structures appear. We assign the value of $T_0 = 12$ K by looking at the temperature at which the difference between the two curves becomes equal to the statistical error.

Unlike $\langle Q_4 \rangle$, the probability distribution $\omega(Q_4)$ is not a good discriminator for solidlike and liquidlike states. This means that the values of Q_4 for liquids and solids overlap substantially. An immediate consequence is the impossibility to estimate the free energy barrier that separates both phases in the melting region. A way to judge the free energy barrier is by calculating the Landau free energy $\phi(Q_4)$ which is related to $\omega(Q_4)$ by the following formula:[38]

$$\omega(Q_4) = \exp\{-N\beta[\phi(Q_4) - f]\}, \tag{12}$$

where f is the Helmholtz free energy. Figure 10 shows $\phi(Q_4)$ for a few temperatures across the melting region. No two minima are ever formed due to the overlap.

VII. CONCLUSIONS

In this paper we have characterized the canonical phase changes of the water octamer by using parallel tempering Monte Carlo simulations in combination with the multihistogram method. We have showed that the parallel tempering algorithm is successful in overcoming problems of ergodicity breaking in a complex molecular system. The parallel tempering method substantially reduces the correlations in the melting region in comparison with standard Metropolis Monte Carlo.

The peak in the heat capacity is a good indicator for the solid–liquid transition. This peak, is very well determined by the use of the multihistogram algorithm. We have found the melting temperature $T_{\max}=178.5$, which is in good agreement with previous studies. A shoulder in the heat capacity at lower temperatures suggests a solid–solid phase change. However, this quantity is not sensitive enough to fully characterize this transition.

We have studied an order parameter to monitor the phase change at low temperature. This parameter $\langle Q_4 \rangle$, together with the probability $p_b(T)$ that different basins are visited, is able to locate the onset of the first phase change at $T_0 = 12$ K. For temperatures below T_0, we have only the isomer D_{2d}. Above T_0, a mixture of the isomers D_{2d} and S_4 is present.

The dependence of the phase changes on the size of the cluster can provide insights into the nature of the bulk phase transitions. We have shown that the parallel tempering method in combination with the multiple histogram algorithm is a successful tool to investigate the phase changes in these complex systems. An extension of this work to larger clusters is currently underway. Initial results for c_v as a function of temperature for $(H_2O)_{12}$ and $(H_2O)_{16}$ indicates the feasibility of this approach.

ACKNOWLEDGMENT

Partial financial support from NSF (CHE 9733189) is gratefully acknowledged.

[1] J. Jellinek, T. L. Beck, and R. S. Berry, J. Chem. Phys. **84**, 2783 (1986).
[2] R. S. Berry, T. L. Beck, H. L. Davis, and J. Jellinek, Adv. Chem. Phys. **70B**, 75 (1988).
[3] R. S. Berry, Nature (London) **393**, 212 (1998).
[4] R. S. Berry and D. J. Wales, Phys. Rev. Lett. **63**, 1156 (1989).
[5] R. S. Berry, Microscale Thermophys. Eng. **1**, 1 (1997).
[6] D. J. Wales and R. S. Berry, Phys. Rev. Lett. **73**, 2875 (1994).
[7] R. E. Kunz and R. S. Berry, Phys. Rev. Lett. **71**, 3987 (1993).
[8] R. S. Berry, in *Theory of Atomic and Molecular Clusters with a Glimpse at Experiments*, edited by J. Jellinek (Springer, New York, 1999), pp. 1–26.
[9] C. J. Tsai and K. D. Jordan, J. Chem. Phys. **95**, 3850 (1991).
[10] C. J. Tsai and K. D. Jordan, J. Chem. Phys. **99**, 6957 (1993).
[11] J. Pedulla and K. Jordan, Chem. Phys. Lett. **239**, 593 (1998).
[12] D. Wales and I. Ohmine, J. Chem. Phys. **98**, 7245 (1993).
[13] A. Vegiri and C. S. Farantos, J. Chem. Phys. **98**, 4059 (1993).
[14] J. Rodriguez, D. Laria, E. J. Marceca, and D. A. Estrin, J. Chem. Phys. **110**, 9039 (1999).
[15] C. J. Tsai and K. D. Jordan, J. Phys. Chem. **97**, 5208 (1993).
[16] P. N. Day, R. Pachter, M. S. Gordon, and G. N. Merrill, J. Chem. Phys. **112**, 2063 (2000).
[17] J. Kim, B. J. Mhin, S. J. Lee, and K. S. Kim, Chem. Phys. Lett. **219**, 243 (1994).
[18] C. Lee, H. Chen, and G. Fitzgerald, J. Chem. Phys. **102**, 1266 (1994).
[19] C. J. Gruenloh, J. R. Carney, C. A. Arrington, T. S. Zwier, S. Y. Fredericks, and K. D. Jordan, Science **276**, 1678 (1997).
[20] D. A. Estrin, L. Paglieri, G. Corongiu, and E. Clementi, J. Phys. Chem. **100**, 3701 (1996).
[21] U. Buck, I. Ettischer, M. Melzer, V. Buch, and J. Sadlej, Phys. Rev. Lett. **80**, 2578 (1998).
[22] W. B. Blanton, S. W. Gordon-Wylie, G. R. Clark, K. D. Jordan, J. T. Wood, U. Geiser, and T. Collins, J. Am. Chem. Soc. **121**, 3551 (1999).
[23] D. D. Fratz, D. L. Freeman, and J. D. Doll, J. Chem. Phys. **93**, 2769 (1990).
[24] E. Marinari and G. Parisi, Europhys. Lett. **19**, 451 (1992).
[25] M. E. J. Newman and G. T. Barkema, *Monte Carlo Methods in Statistical Physics* (Oxford University Press, Oxford, 1999).
[26] J. P. Neirotti, F. Calvo, D. L. Freeman, and J. D. Doll, J. Chem. Phys. **112**, 10340 (2000).
[27] F. Calvo, J. P. Neirotti, D. L. Freeman, and J. D. Doll, J. Chem. Phys. **112**, 10350 (2000).
[28] M. R. Ghayal and E. Curotto, J. Chem. Phys. **113**, 4298 (2000).

[29] E. Curotto, J. Chem. Phys. **114**, 4533 (2001).
[30] O. Matsuoka, E. Clementi, and M. Yoshimine, J. Chem. Phys. **64**, 1351 (1976).
[31] N. Metropolis, A. W. Rosenbluth, M. N. R. A. H. Teller, and E. Teller, J. Chem. Phys. **21**, 1087 (1953).
[32] M. P. Allen and D. J. Tildesley, *Computer Simulation of Liquids* (Oxford University Press, Oxford, 1987).
[33] A. M. Ferrenberg and R. H. Swendsen, Phys. Rev. Lett. **63**, 1195 (1989).
[34] K. Binder and D. W. Heermann, *Monte Carlo Simulation in Statistical Physics* (Springer, New York, 1997).
[35] H. Flyvbjerg and H. G. Petersen, J. Chem. Phys. **91**, 461 (1989).
[36] S. Mignani and R. Rosa, Comput. Phys. Commun. **92**, 203 (1995).
[37] P. J. Steinhardt, D. R. Nelson, and M. Ronchetti, Phys. Rev. B **28**, 784 (1983).
[38] R. M. Lynden-Bell and D. J. Wales, J. Chem. Phys. **101**, 1460 (1994).
[39] J. P. K. Doye, M. A. Miller, and D. J. Wales, J. Chem. Phys. **110**, 6896 (1999).